STATIC ENERGY ABSORPTION CAPACITY OF GRAPHITE-EPOXY TUBES

Michael W. Hyer and Marc R. Schultz

Department of Engineering Science and Mechanics
Virginia Polytechnic Institute and State University, Blacksburg, VA 24061, USA

SUMMARY: This paper examines the energy absorption capacity of Akzo Nobel Fortafil 50k carbon fiber composite tubular specimens crushed axially in a quasi-static fashion. Round and square tubular specimens with ±45° and ±45°/0° constructions were studied. As a comparison, similar tubular specimens were fabricated using T300 12k fiber, an aerospace standard. The towpreg form of these materials, obtained from Thiokol TCR Composites Division, was filament wound to produce specimens. The fundamental issue was to study the energy absorption capacity of the lower cost 50k material in comparison to the 12k material, and to determine the influence of specimen geometry and fiber orientation schemes on the energy absorption capacity.

KEYWORDS: crashworthiness, specific energy absorption, load ratio, crushing characteristics, low cost, tubes

INTRODUCTION

While there already exists a significant body of literature regarding the energy absorption capabilities of fiber-reinforced composite materials (for example, see refs. 1-3), new material developments and manufacturing schemes require a continuing investigation of the problem. Though previous studies have concluded that graphite-reinforced materials often absorb energy better than glass- or Kevlar-reinforced materials, the cost of graphite is considerably higher. However, carbon fiber that is lower in cost than traditional aerospace-grade carbon fiber is being marketed and offers some potential for cost-conscious industries. Additionally, other developments have made the manufacture of composite components somewhat simpler. Specifically, for filament winding, pre-impregnated tow (towpreg) is available that can be used to wind structural components. Towpreg is a material that consists of fiber bundles, or tows, that have been pre-impregnated with a matrix material, and offers an alternative to wet winding that is attractive because there is no need for an open resin bath and the associated cleanup. However, the lower cost materials have a higher number of fibers per tow, and therefore are, by their nature, coarser than their aerospace-grade counterparts. They, therefore, could result in different energy absorption characteristics and this must be considered. Of course, with the higher tow count material the variations in fiber orientation scheme, specimen geometry, and crushing speed are still important. With these issues in mind, the specific objective of this research effort was to compare the energy absorption capacity of tubes fabricated with lower cost, high tow count graphite fiber with tubes fabricated with a more expensive aerospace-grade graphite

fiber. Different fiber orientation schemes, different specimen geometries, and static and dynamic testing were considered. This paper deals only with the static energy absorbing characteristics. The dynamic effects will be discussed in a subsequent paper.

To meet the specific objectives, two types of epoxy-matrix towpreg material were obtained from the Thiokol TCR Composites Division. The first type was T300 12k carbon fiber, an aerospace standard, which cost $54 per kilogram in towpreg form. The second type was Akzo Nobel Fortafil 50k carbon fiber which cost $33 per kilogram of towpreg. Both of these materials were used to filament wind round and square cross-section tubes with only ±45˚ fibers and tubes with both ±45˚ and axial (0˚) fibers. The tubes were cut into shorter specimens which were then crushed axially.

An important parameter when characterizing energy absorption capacity is the energy absorbed per unit mass of crushed material, called the *specific energy absorption*, or SEA. Another important parameter is the shape of the crush load vs. crush length relation. Figure 1 shows an ideal relation. As the crushing begins, the load quickly rises to a peak value, then drops off slightly and stays relatively constant. In this way the energy absorption is maximized for the length of material crushed. An initial peak load, F_{imax}, much greater than the average crush load, F_a, means large loads are needed to initiate crushing. Generally high initial peaks are undesirable in vehicular energy management situations because large loads would then be imparted on the occupants. The specific energy absorption and the *load ratio*, namely, the ratio of the peak load to the average load, are used here to describe material response of the axially crushed tubular specimens.

SPECIMEN FABRICATION

Two 1.4m long aluminum mandrels were used to manufacture of 840 mm tubes that were subsequently cut into shorter specimens. The mandrels were slightly tapered to facilitate the removal of the finished tube. One mandrel was circular in cross-section with a diameter of about 50 mm. The other mandrel had a square cross section that was about 62 mm per side. The corners of the square mandrel had a radius of 12.7 mm. Three specimens for crushing were cut from each 840 mm tube: either two static specimens and a single dynamic specimen, or two dynamic specimens and a single static specimen. The single specimen was always cut from the middle of the 840 mm long tube. A 30˚ external bevel, used as a crush initiator, was ground into the smaller end of each slightly tapered specimen.

To obtain approximately the same wall thickness for each fiber type the ±45˚ 12k tubes were wound with eight ±45˚ layers, while the 50k tubes were wound with four ±45˚ layers. For the tubes with 0˚ layers, the fiber orientation scheme for the 12k tubes was $[\pm45^\circ/0^\circ/\pm45^\circ/0^\circ/\pm45^\circ/\pm45^\circ/0^\circ/\pm45^\circ/0^\circ/\pm45^\circ]_T$, while the fiber orientation scheme for the 50k tubes was $[\pm45^\circ/0^\circ/\pm45^\circ/0^\circ/\pm45^\circ]_T$.

The tubes were consolidated using shrink wrap. The ends of the consolidated tubes were trimmed with a diamond-bladed band saw and trued with a disc sander. Each tube was then weighed and its volume and all the relevant dimensions measured. Each tube was subsequently cut into shorter specimens with the band saw. The sander was used to true the ends of the specimens and apply a 30˚ bevel crush initiator to the smaller end of each specimen. Each specimen was also individually weighed and measured for relevant dimensions, both before and after the bevel was applied.

As each specimen was cut from a longer tube, it was given a specimen designation which was a code that identified the specimen geometry, fiber orientation scheme, fiber type, and indicated from which 840 mm tube it was cut and from where along the length of that tube it was cut. The first character of the designation identified the cross-sectional shape: “c” for circular cross section, “s” for square cross section. A “z” in the second position indicated that tube has the fiber orientation scheme with the 0˚ layers in it. Next, the number “12” or “50” indicated whether the tube has the 12k T300 or 50k Fortafil fiber tows. For each set of tube parameters, i.e., circular or square, 12k or 50k, two or three tubes were manufactured that were intended to be replicates, and the “.#” indicated the number of the replicate tube. For cases where three replicate tubes were manufactured, the first tube was used to optimize the manufacturing process and conduct preliminary testing. The two dynamic or two static specimens cut from the 840 mm tube were cut from the ends and given the suffix “a” or “b,” with the “a” specimen coming from the larger end and the “b” specimen coming from the smaller end of the slightly tapered tube. The designation was not amended for the singular specimen cut from the middle of the tube. Here it should be noted that the first five 50k tubes manufactured (c50.1, c50.2, cz50.1, s50.1, sz50.1) had a wider tow spacing than the last four 50k tubes (c50.3, cz50.2, s50.2, sz50.2). This was due strictly to the lack of familiarity with the higher fiber count tows and not due to the material itself. Adjustments to the filament winder parameters eliminated the problem of the wider tow spacing for the last four tubes.

TUBE AND SPECIMEN PHYSICAL CHARACTERISTICS

For each uncut 840 mm tube the following measurements were made: inner and outer diameters (inner and outer square side-lengths for the square tubes), length, mass, and volume. For each specimen cut from an 840 mm tube the following measurements were made: inner and outer diameters (inner and outer square side-lengths for the square tubes), length, mass, and wall thickness. The inner and outer diameters and square side-lengths were measured at two locations on each end of the uncut tubes and resulting specimens. Lengths were measured in four places and masses were measured twice. The wall thicknesses of the circular geometries were measured in four places on each end, while the wall thicknesses of the square geometry tube specimens were measured in eight places on each end. The wall thicknesses on the square geometry tubes were measured on each flat and corner of each end of the square geometries because the square tubes were thinner in the corners than on the flats.

Regarding the volume measurements: for the 12k tubes there was fairly good consistency between replicate pairs. The effect of the tow spacing for the 50k tubes, mentioned above, was evident in the volume data. Regarding the mass data: the mass per length of the “a” specimen was, as expected, greater than that of the “b” specimen because the tapered mandrel had larger dimensions on the “a” end. The mass per length was more consistent for the 12k tubes than for the 50k tubes, the 50k tubes again reflecting the effect of the change in tow spacing. The walls of the 12k circular specimens were all thicker than the walls of the 12k square specimens. The wall thicknesses for the 50k specimens were not as uniform as those of the 12k specimens, and there did not seem to be a trend with the circular vs. square specimens. For the most part, all of the 50k specimens were thicker than their corresponding 12k counterparts. Also, for all square specimens the thickness in the corners was less than the thickness of the flats. This is indicative of higher compaction pressure in the corners.

TESTING AND REDUCTION OF DATA

The axial crush tests were done on an Instron model 4206-006 displacement-control machine with a 44.5 kN load cell. The cross-head speed was set at 6.35 mm/minute. The specimens were crushed approximately 100 mm. The crush load and cross-head displacement were recorded as a function of time. The energy absorbed during crush was calculated by integrating under the crush load vs. crush length (cross-head displacement) relation. The average crush force sustained over a specific crush length was calculated continuously as the tube was crushed. To obtain the SEA, the energy absorbed during crush was divided by the mass of the crushed material. To calculate the load ratio, the value of the crush load at the initial peak was divided by the final average crush load, F_{imax} and F_a, respectively, in Fig. 1.

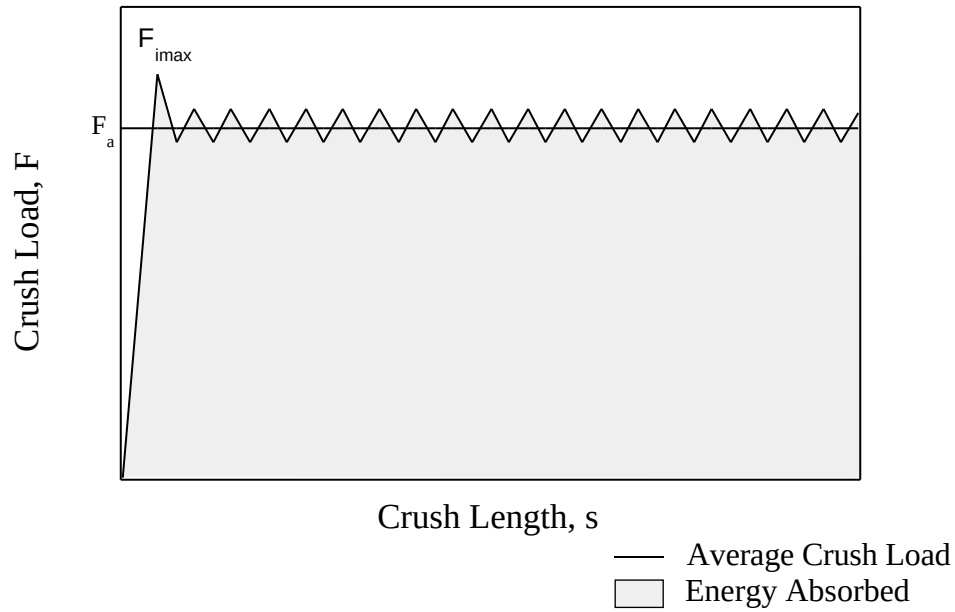

Fig. 1 - Ideal crush load vs. crush length relation

ENERGY ABSORPTION CHARACTERISTICS

In all, 24 static specimens were tested. The tests provided information regarding the influence of specimen geometry, fiber angles, and tow size on specific energy absorption. These findings are discussed below.

CRUSH MODES OBSERVED: There were several different modes of stable crushing observed. In all the modes the walls of the tube were split part way through the thickness, and the inside portion of a wall was pushed, or folded, to the inside of the tube and the outside portion was pushed and bent outward. Between the portion that was pushed inward and the portion that was pushed outward there was a debris wedge. This wedge consisted of pulverized material and probably helped to split the wall. With the *tearing* mode the portion of the wall that was folded outward was torn in several places by hoop stresses. Between these tears the wall was still intact but had matrix damage. These sections between the tears are often referred

to as *fronds* and are shaped and positioned like flower petals. In the *splaying* mode most of the individual tows were separated, something like delamination, but on a tow-by-tow basis. Often the tows were further split by matrix cracks running parallel to the fibers. These two modes are variations on those observed and identified by Farley and Jones [2] and by Hull [3]. In the *socking* mode the outside portion of the wall that was folded outward stayed together but was pushed back over itself, similar to the way a sock comes off the foot when the sock is pulled downward from the top and out, over the foot part of the sock. Often these failure modes were combined to the point that two or all three would be seen in a single specimen.The socking mode for a 12k circular specimen with 0˚ fibers is illustrated in Fig. 2.

Fig. 2 - Socking crush mode

DETAILS OF THE 12k SPECIMENS: A typical crush load vs. crush length trace for a 12k specimen is shown in Fig. 3. The solid line is the measured crush load vs. crush distance, while the broken line represents the crush load averaged over the crush length. This trace is for a circular specimen and it approximates the ideal trace of Fig. 1 in that the trace representing the measured load stays relatively constant once it has made the transition from the zero load condition. The measured load trace did, however, have two or three non-distinct initial peaks and large valley-to-peak variations that are not considered ideal.

The SEAs for the 12k specimens are seen in Fig. 4. In this figure the two columns together represent the SEAs of the specimens cut from the ends of the 840 mm tubes (the “a” and “b” specimens), with the dark column representing the “a” specimen and the light column representing the “b” specimen. The columns that stand alone represent the SEA of the single specimens cut from the middle of the 840 mm long tubes. It is seen that all of the circular 12k specimens had higher SEAs than their corresponding square 12k specimens. It is also seen that the “a” and “b” specimens had higher SEAs than the specimens from the middle of the 840 mm tubes for all of the 12k static tests. It seems that the 0˚ layers had little effect on the SEA. Also shown in Fig. 4 are the crush modes observed for each crushed specimen. The crush modes that occurred in each specimen are shown on top of the column for that specimen: “t” for the tearing mode, “sp” for the splaying mode, and “so” for the socking mode. All of the crushing modes described earlier were observed with the 12k specimens. The 12k circular specimens with the

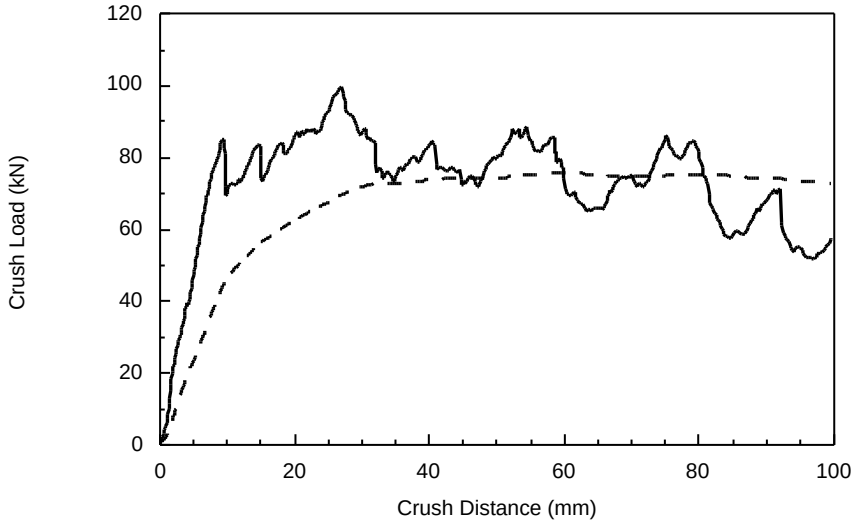

Fig. 3 - Typical crush load vs. crush length trace for 12k specimen

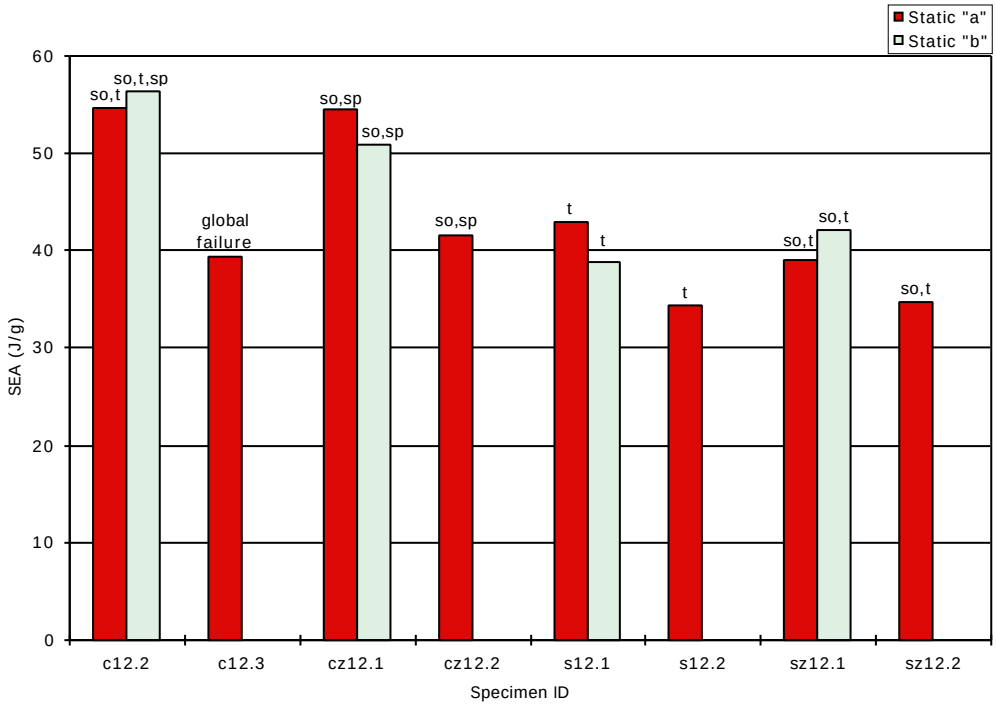

Fig. 4 - Specific energy absorption (SEA) and crush modes for the 12k specimens

0˚ layers all failed primarily by the socking and splaying modes. All of the 12k square specimens failed by tearing into four fronds with little splaying. The tearing occurred at the radiused corners, and each flat stayed intact but exhibited matrix cracking. The 12k square specimens with the 0˚ layers also showed a moderate amount of socking.

To explore the difference in SEA between the end and middle specimens, normalized values of

thickness, linear density, and SEA for each specimen were created. The values were normalized by dividing the value from the particular specimen by the value from the corresponding "a" specimen. In this way each set of three replicate specimens were normalized by the first one in the set. Based on the normalized data, it is believed that there were variations, other than just the taper, along the lengths of the 840mm uncut tubes. Perhaps the ends were more well-consolidated or the fiber architecture in the ends was slightly different than the architecture in the middle due to the turnaround zone of the filament winder at each end of a tube.

The load ratios for the 12k specimens are seen in Fig. 5. The load ratios for the circular specimens, except for specimen c12.3, were between 1 and 1.2, while the load ratios for the square specimens were between 1.2 and 1.6.

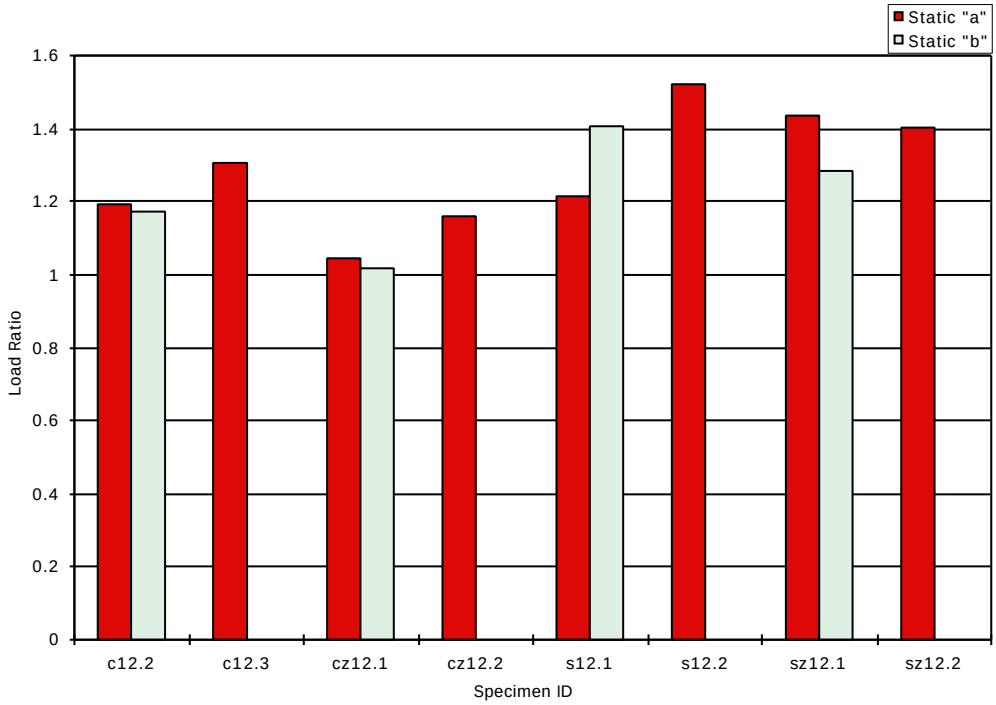

Fig. 5 - Load ratios for the 12k specimens

DETAILS OF THE 50k SPECIMENS: A typical crush load vs. crush length trace for a 50k specimen is shown in Fig. 6. This trace is for a square specimen with 0° fibers. The 50k traces generally showed more deviation from the ideal trace of Fig. 1 than did the 12k traces. The 50k specimens also often showed dual initial peaks and those peaks were not always the highest of the trace. However, the valley-to-peak variations were smaller than for the 12k specimens.

It is seen from Fig. 7 that all of the specimens from the 840 mm tubes with the tighter tow spacing (c50.3, cz50.2, s50.2, and sz50.2) had higher SEAs than their counterparts with the wider tow spacing. The circular specimens with the 0˚ layers had the highest SEAs of the 50k specimens. The presence of the 0˚ layers seemed to increase the SEAs for the 50k circular specimens, but the 0˚ degree layers seemed to have no effect on the SEAs of the 50k square specimens. The SEAs of the square specimens were, for the most part, lower than the SEAs of the circular specimens.

The crush modes are given for each specimen in Fig. 7 above the column that represents that

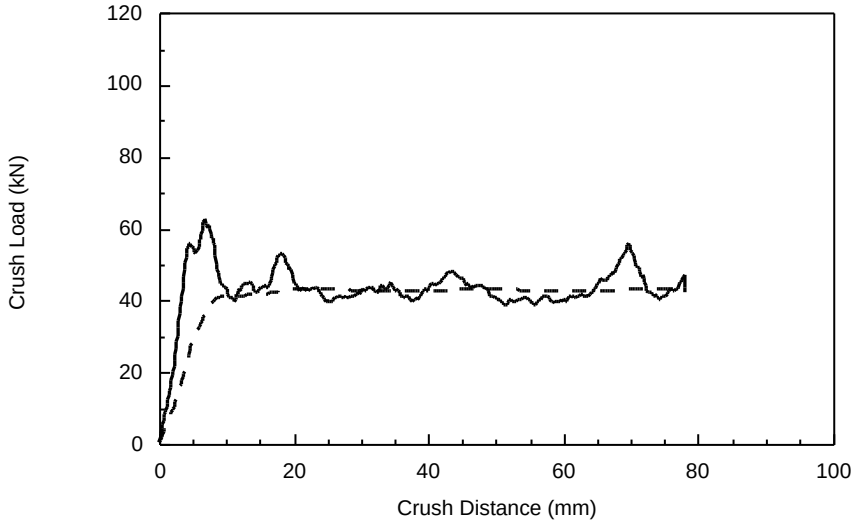

Fig. 6 - Typical crush load vs. crush length trace for 50k specimen

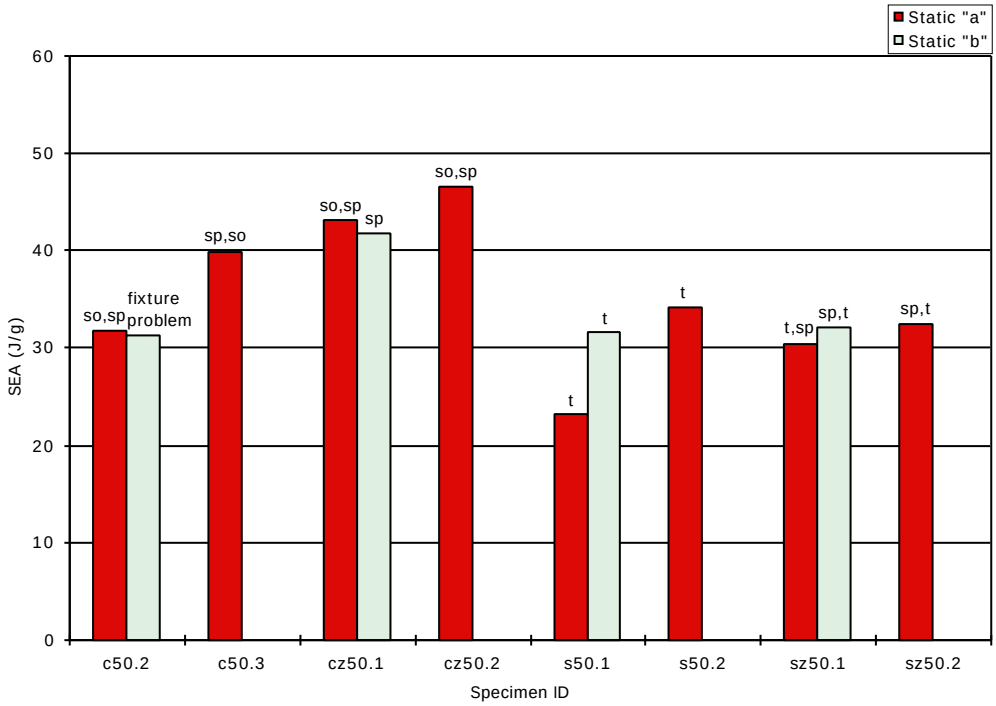

Fig. 7 - Specific energy absorption (SEA) and crush modes for the 50k specimens

specimen. The 50k round specimens failed mostly by the splaying mode. All of these specimens, except for specimens c50.2b and cz50.1b, also showed socking. The square 50k specimens failed primarily by tearing into fronds and splaying. With the square 50k specimens there also seemed to be more tows that fractured after being separated than with the other specimens, either circular 50k specimens or any of the 12k specimens (i.e., the splayed tows were short due to fiber breakage). The square specimens with the 0˚ layers seemed to separate into indi-

vidual tows much more than the other 50k square specimens to the extent that it was hard to distinguish the fronds.

The load ratios for the 50k specimens are shown in Fig. 8. The load ratios for the circular 50k specimens were generally lower than those for the square specimens. Three of the four 50k specimens with the tighter tow spacing (c50.3, cz50.2, and s50.2) had lower load ratios than at least one of the corresponding specimens with the wider tow spacing.

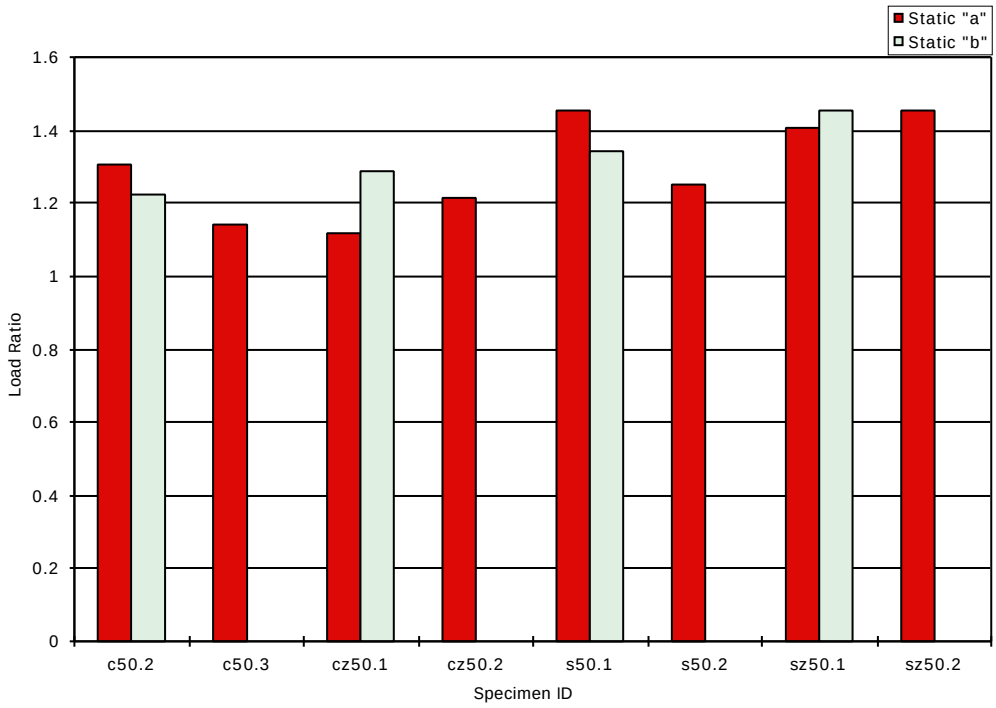

Fig. 8 - Load ratios for the 50k specimens

COMPARISONS BETWEEN 12k AND 50k SPECIMENS: Overall, the 50k specimens showed smaller valley-to-peak variations in the crush load vs. crush distance traces than did the 12k specimens. The circular 12k specimens seemed to have the largest variations. When looking at figures of the SEAs (Figs. 4 and 7), the 12k and the 50k specimens show an opposite trend. For the 12k specimens, both end specimens (“a” and “b”) for one 840 mm tube had higher values of SEA than did the single middle specimen from the other 840 mm tube. The reverse was true for the 50k specimens; the single 50k specimen always had a higher value of SEA than did either of the corresponding end specimens. Because both of the 840 mm 12k tubes within a family were fabricated in the same manner, it is postulated that the difference in the SEAs was due to the position along the tube from which the specimen was cut. This same comparison cannot be made with the 50k specimens because the tubes from which the middle specimens came had the decreased tow spacing.

The 12k end specimens had much larger values of SEA than the matching 50k end specimens. The 12k single middle specimens and the matching 50k single middle specimens, however, had fairly close SEAs, with the SEA for only one of the 50k single middle specimens being lower than its 12k counterpart.

For both the 12k and 50k specimens, the square specimens had lower SEAs. The square speci-

mens also failed primarily by tearing in the corners. It can then be said that the SEA was lower for the square specimens because either the tearing mode is not as effective at absorbing energy as the other modes, or because the square specimens were somehow inferior in quality to the circular specimens. The tearing in the square specimens occurred mostly in the corners, so not as much percentage of material was used in energy absorption. Also, the square specimens showed large voids in the flats which may have indicated poor consolidation, so the failure that did occur in the flats may not have absorbed much energy.

The square specimens of both the 12k and 50k material had load ratios higher than 1.25, perhaps too high. Most of the circular specimens of both the 12k and 50k material had load ratios less than 1.25. Of course, the validity of these quantities must be questioned because of the large valley-to-peak variations and the non-distinct initial peaks.

Although some of the results may have been clouded by questions about differences between the end and middle specimens, and the change in tow spacing to improve the quality of the 50k specimen, no obvious disadvantage to using 50k tows for energy absorption was seen.

CONCLUSIONS

Presented have been the results of a study to compare the static energy absorption capacity of low cost 50k carbon fiber tubular specimens with tubular specimens made with more conventional 12k carbon fiber. Wider tow spacing in some of the specimens and possible differences in fiber architecture in the turnaround zones of the filament winder masked possible differences in the specimens made from the two materials. However, it can be said that there were no obvious decreases in energy absorption capacity of the specimens fabricated with the 50k material, and when cost is considered, the 50k material may be the material of choice.

ACKNOWLEDGMENTS

The authors appreciate the support of the NSF Science and Technology Center on High Performance Polymeric Adhesives and Composites at Virginia Tech. The helpful comments from Scott Lindsay and Leo Erickson of Thiokol are also appreciated.

REFERENCES

1 - Mamalis, A.G., Manolakos, D. E., Demosthenous, G. A., and Ioannidis, M. B. *Crashworthiness of Composite Thin-Walled Structural Components*, Lancaster, PA: Technomic, 1998.

2 - Farley, G.L. and Jones, R.M. “Energy Absorbing Capability of Composite Tubes and Beams,” NASA TM 101634, AVSCOM TR 89-B-003, Sept. 1989.

3 - Hull, D. “Energy Absorption of Composite Materials under Crash Conditions,” *Proceedings of the Fourth International Conference on Composite Materials (ICCM IV)*, vol. 1, pp. 861-870, 1982